HIGH LEVEL MODELING IN OPTOELECTRONIC SYSTEMS: TRANSMISSION LINE APPLICATION

Fatima Zohra Baouche[a,b], Farida Hobar[b], Yannick Hervé[a]*

[a] InESS laboratory, Telecom Physic Strasbourg, parc d'innovation, Bld S.Brant 67400 Illkirch Cedex, France.
[b] Laboratory of Microsystems and Instrumentations (LMI), University of Constantine, Route Ain- El- Bay 25000, Algérie.

ABSTRACT

This paper presents different VHDL-AMS modeling techniques to create and improve operational models of optoelectronic components, such as vertical cavity surface emitting lasers (VCSELs) and multimode optical fibers. Our models are designed for designers and developers of optoelectronic transmission systems and intended not to replace the models created with specialized software in the domain of optics and optoelectronics but to help system designers to model the physical level. The modeling technique used is the progressive "top-down" approach; it serves to describe lows-levels abstraction in terms of highs-levels abstraction. We have modeled one by one the physical phenomena of each system component by introducing the main disturbances such as noise in the VCSEL, and fiber attenuation effects for knowing the influence of parasites parameters and transmission limitations according to the length of each fiber type. Our objective is to construct a globally accurate model taking into account the multidisciplinary effects that make up the entire optoelectronic transmission line including electrical, thermal and optical behaviors and to find the method to integrate them into a modern design tool. The simulation results are positively compared with models results published in literature.

KEYWORDS: *VHDL-AMS; VCSEL; graded-index fiber; step-index fiber.*

I. INTRODUCTION

The evolution of electronics was led by the objective of creating systems of increasing computational power. Electronics evolves in terms of improved processing power, enhanced miniaturization and the important possibility of autonomy while minimizing research and production costs. Today, systems are no longer exclusively electronic, and the needs of research are increasing by moving from a circuit-based to a system-based approach. These evolutions involve the simultaneous implementation of multiple types of technologies, such as electronics, mechanics, optics and chemistry. These multi-domain systems open new possibilities but also pose additional challenges in managing the complexity and heterogeneity of their design. The design community now adheres to the MBD (Model-Based Design) approach [1]. The optimization difficulties of the design process are increased by "Time to Market" considerations, which forces a re-evaluation of classical methodology and the development of new modeling approaches. We must reconsider high-level verification, functional modeling, reuse, and module management of intellectual property (IP) [2] for multidisciplinary systems. These approaches must also be considered from the first steps of design.
The modeling language that is sufficiently mature to model and simulate our system is VHDL-AMS (Analog and Mixed-Signal-AMS language) IEEE Standard 1076.1-2007 [2-3]. This language allows for equal treatment of a logical model, an analog model or a mixed-model [4-5] within the same component or system. The design method that we used is the "top-down" approach [2,6]. This approach

starts from an outside vision of the device, and, with each analysis step, it delves deeper into a detailed view of the system. We continue until we have reached a level of detail sufficient for understanding our objectives. Once the specifications are established, the modeling begins with a behavioral level that describes the system as a "black box" [7] and then descends gradually into the abstraction levels according to our needs. It is necessary to ensure the formalization, capitalization and reuse of the models that are developed. We must also be able to store the models in well-documented libraries of generalist components. This approach will save development time by eliminating the need to "create the model" for each new system, instead requiring only improvements to an existing model.
Our goal is to develop a VHDL-AMS documented library of optoelectronic component models that can be used in the models of an optical transmission system and take into account the inherent constraints in the various domains and the interactions between them. The study of this system requires the development of complex multidisciplinary generic models that consider the electronics, optoelectronics, optical, and thermal domains.

II. VHDL-AMS METHODOLOGY

2.1 Modeling Steps

In the design of multidisciplinary systems, several steps must be considered. The first step is to determine the potential needs of a client and perform a problem analysis. Following the analysis, we prepare the requirement specification. This specification poses the problems, the constraints imposed on the solution, and the criteria used to judge the design quality. In posing the problem, all required functions and desired characteristics must be specified. We then generate the possible solutions; this step is often called the "design step." The solutions are prepared in sufficient detail to indicate how to obtain each of the desired functions. The different solutions are evaluated, and the most suitable one is chosen. In the final step, "implementation," the work is performed with the selected solution to determine the optimal design details. Once these steps are completed, we have a library of VHDL-AMS models that describe all or part of a system.
The need to accurately predict the performance of components requires a physical modeling approach and the development of predictive models [8]. The models developed in our work are based on the physical equations of components using their internal parameters. The behavioral description is a mandatory step in device design. It translates the system characterizations into a «simulated specification» that reproduces the functioning system by establishing relationships between inputs and outputs as if it were a "black box." It is rare that the objectives of a project are satisfied by the behavioral simulation of a device. We must then remove the cover of the "black-box" of the system to observe its internal functioning and isolate its physical or functional constituent groups. This approach is not a modeling level as defined in the simulation but rather the conceptual meaning of a model. The structural analysis [9-10] establishes the links between the blocks constituting the system, regardless of their behavioral or physical implementation. The development of these models requires the intervention of many domains of expertise. The physics specialists must develop the mathematical models to better report the operational subtleties of the components. The language specialists must find the best information technology solution suited to the processing of the physical model.
To simulate the complete system, we must make connections between the models that are necessary for our simulation using the component instantiation method; thus, we take the more efficient copy of the models already documented in our work library. To instantiate the transmission block, we use the parameter copy of the current generator model, a copy of the resistance model and a copy of the VCSEL model at the abstraction level chosen. Then, we configure and connect each one of these copies to its respective environment. In this study, the instantiation is used in the direct form (this approach is well explained in [2]). The instantiation is performed for each block of the optical link by connecting the output of each block with the input of the next block, and so on, until we group all blocks of the complete system. The VCSEL modeling is based on studies performed by I. Kenichi et al. [11-12], and from the models created for other studies [13-20]. These studies allow us to rewrite the new models of the VCSEL and of the optical fiber using the top-down approach.

2.2 Simulation setup

The fact that both modeling approaches can be implemented in VHDL-AMS and thus fit into an electronic design flow is important from a practical point of view because it allows a designer to use standard modeling and simulation tools. A number of various commercial VHDL-AMS simulators are currently available from several electronic design automation companies.

The numerical computation of differential equations and the simulation of the analog and mixed aspect of our models are performed using the simulator Smash 5.17 from Dolphin Integration which supports most of IEEE standard VHDL-AMS, but the models are reusable with other tools due to the standardization of the language. The examples given below have been written accordingly and targeted to compile and run on this particular simulator. Porting them to another simulator may require some modifications depending on the VHDL-AMS language support of the simulator.

The design hierarchy allows to define a test-bench consists of concurrent or simultaneous instructions and components instantiation. This definition is recursive since the components are themselves defined by the same constructions. Terminal components of the hierarchy can be defined by executable instructions, ie simultaneous instructions and/or competitors. Prepare the models for simulation pass by the elaboration phase. This is the time the constants and the generic parameters are fixed and the description hierarchy allows recover the good models in the Resource Library. At that time all competitors instructions (Boolean equations) are reduced to the same level in a sea of process interconnected and are supported by discrete event simulator and all simultaneous instructions (differential equations) are grouped into a data structure for the analog simulator. The model will be supported mostly by two simulation kernels that we should synchronize. The analog simulator produces the ASP (Analog Simulation Point) while the digital simulator produces the LSP (Logic Simulation Point). Representation hierarchy is therefore a view to facilitate the approach of the human designer, but it is of no use for simulation environment. We use the design hierarchy to optimize the computational time.

III. SIMULATION RESULTS AND DISCUSSION OF VCSEL MODELS

In the last decade, the VCSELs appeared as a reliable low-cost high-speed solution for data communication applications and interconnects [13,21-22]. Many studies [17,23] have confirmed that the dynamic characteristics of the single-mode VCSEL are similar to those of a device with two modes. In this study, we limited the VCSEL model to operation in single-mode. Our calculations are based on the photon total number and not on the photon's distribution between the transverse modes. The wavelength used is constant and equal to the nominal wavelength indicated by the manufacturer (850 nm).

The engineer responsible for designing a multidisciplinary system can rely on component libraries to lead a project from its definition to its realization while leveraging his experience. To start this demonstration, we reused the VCSEL model already created by [14] using some physical equations reported in [24]. We improved it by rewriting its code and adding other physical equations compatible with our specifications set. To write the first model of the VCSEL, we used the rate equations, translating the changes of the carriers and photon number in the laser cavity as previously reported [15]. We completed our model with the equation linking the photon number to the output optical power cited in [16].

3.1 Static and dynamic response of the VCSEL

First, we modeled the VCSEL laser diode in DC to find its main static characteristics, such as the evolution of the carrier and photon number, the voltage across the active layer and the emitted power versus the bias current (see Fig. 1). We saw that, under the emission threshold (I_{th} = 1.5 mA), no optical power was emitted and that the carrier number was proportional to the injection current. However, when Id was greater than I_{th}, lasing commenced, and the carrier number N stabilized to a constant value Nth at the lasing threshold. In addition, the photons number S and the optical power P_{opt} increased almost linearly. Fig. 1(d) shows the light output power versus injected current, which is equal to 2.4 mW for 8 mA. The threshold current is I_{th} = 1.5 mA, and the differential quantum efficiency is $\Delta P_{opt}/\Delta I$ = 0.12 W/A. The VHDL-AMS simulation results for the VCSEL static response are similar to those demonstrated by other researchers [17,25].

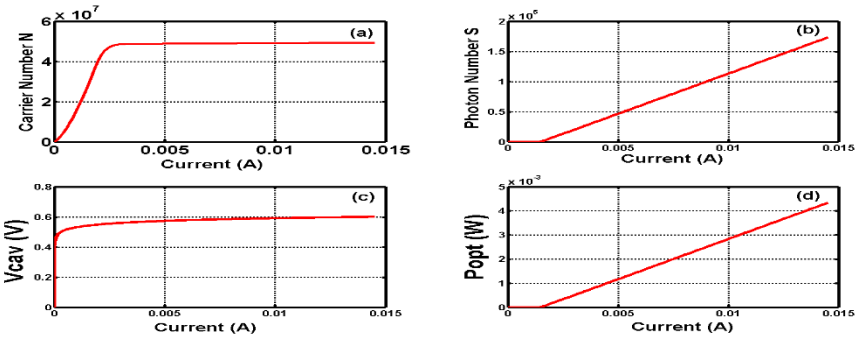

Fig. 1. VHDL-AMS simulation results of the VCSEL static response versus injected current. (a) The carrier number; (b) photon number; (c) voltage in the VCSEL cavity; and (d) output optical power.

To complete the previous model, we studied the VCSEL in the dynamic regime. The injection current is non-static to model the variation of parameters over time. To simulate binary data transmission through an optical fiber, we used a square-pulse electrical signal between 0 and 8 mA as the input current. The binary "1" corresponds to the nominal injection drive current of the device, and the binary "0" corresponds to a current just above threshold, for better separation of the high and low transition levels of the transmitted signal. As shown in Fig. 2, we noted that the complimentary simulation characterizing the VCSEL dynamic behavior was reflected perfectly. Before the injection current reached I_{th}, the energy supplied to the device was used to create carriers (excited atoms). After Id reached I_{th}, the energy supplied was used to emit photons; the laser needed more time to reach the steady state.

The simulation results of the VCSEL dynamic response are similar to those found in the literature. In the paper [15], they used a square current between 20 and 50 mA, but, before reaching its nominal value, the optical power was not stable; it stabilized at 250 ps to a nominal value of 7 mW. In our study, we solved the problem of agreement between the optical power and the current applied, which explains the nonexistence of the optical power leap (see Fig. 2(d)). Our system consumes some energy compared to that of a previous study [15] that used a threshold current (4 mA) larger than the threshold current used in our study.

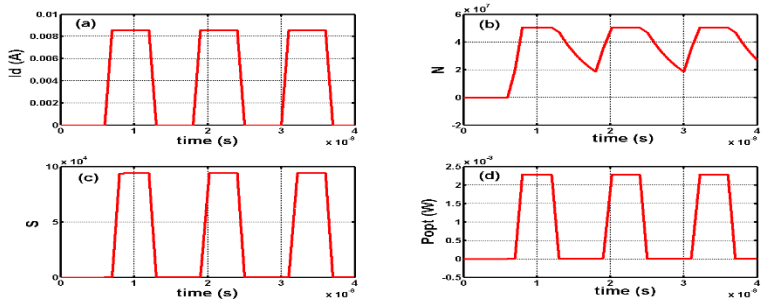

Fig. 2. Simulation results of the VCSEL dynamic response. (a) The injection current; (b) carrier number; (c) photon number; and (d) output optical power.

3.2 Thermal dependence and noise influence of the VCSEL

In accordance with the top-down method, for our model to be more realistic, we modeled the temperature elevation caused by power dissipation, which is equal to the difference between the electrical power consumed and the optical power generated [18]. All parameters of the rate equations of the carrier and photon numbers are dependent on the temperature. Thus, it is necessary that constant parameters of the model become complex physical equations as a function of the temperature; they should also be evaluated at each calculation point. To simulate the VCSEL thermal effect, we add the equations to our model, which provide a basic approximation that includes heat sources, heat flows and the thermal properties of VCSELs, as given by a previous study [18]. The parameters that depend on the temperature variation are the optical power $P_{opt}(T)$ [19], the threshold current $I_{th}(T)$ [26], the wavelength $\lambda(T)$ [15,18], the slope efficiency $\eta(T)$ [27], the effective gap energy Eg (T) and the differential gain G(T) [18,20].

Transient analysis is a crucial part of the design of the VCSEL [28], but the static simulation for several values of the junction temperature is also very important in identifying key factors, such as the threshold current and the maximum output power. The optical powers as a function of the injection current are illustrated in Fig. 3. The threshold current increases for temperature changes between 25 and 65 °C, leading to a decrease in the output power that is maximal at an ambient temperature (T=25 °C). These results are consistent with the curves of measurements provided by the manufacturers of VCSEL, and they show a good agreement with the results reported in several studies [14,29-31].

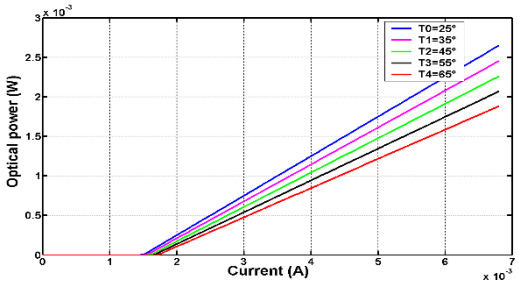

Fig. 3. Simulation results of optical power versus injection current at several temperatures.

Fig. 4 presents the parameter changes of a VCSEL over a range of temperatures from 25 to 130 °C. We noticed that the slope efficiency decreased approximately linearly by $2.5.10^{-3}$ with an increase in the temperature of 1 °C (see Fig. 4(a)). This change was due to the increase in the output optical power with the injection current. According to Fig. 4(d), the wavelength value increases approximately linearly by 0.06 nm for a temperature increase of 1 °C, exactly as in [15,29], although we did not use the same temperature range, in contrast to the gap energy, which decreased slightly by 5.10^{-4} eV with each temperature increase of 1 °C (see Fig. 4(b)). As shown in Fig. 4(c), the optical gain decreased by 12.5 cm-1 for a 1 °C increase in temperature. This decrease was due to the increased threshold current.

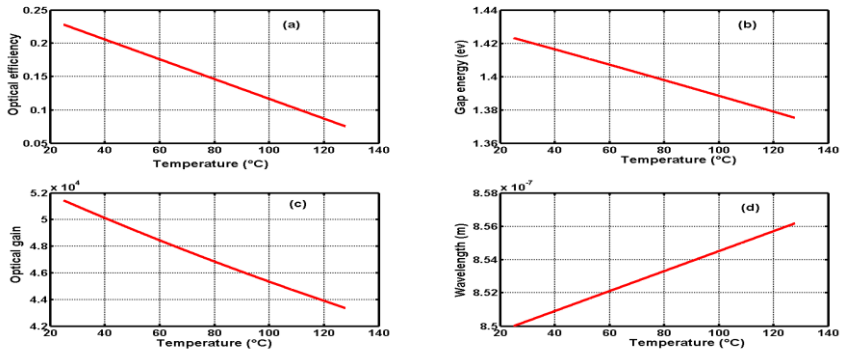

Fig.4. Simulation results of the VCSEL parameter changes with temperature. (a) The optical efficiency; (b) gap energy; (c) optical gain; and (d) wavelength.

The basic mechanisms that contribute to the generation of the noise are spontaneous emission and electron-hole recombination. To account for the laser noise intensity, we added the Langevin forces FN and FS of the electron and photon number fluctuations to rate equations [32-33]. The Langevin forces are described by $F_{N/S} = \sqrt{D_{nn/ss}}\,(X_{1/2})$ [34-35]. D_{nn} and D_{ss} are the diffusion coefficient factors of the carriers and the photons, respectively, corresponding to a noise spectral density associated with each variable [13,32,36]. To simulate F_N and F_S in VHDL-AMS, we generated two random real variables, X_1 and X_2, belonging to the interval [-1, 1] using the "Uniform" function of VHDL-AMS language, which enables us to draw a random value with uniform distributions using a specific formatting scheme to obtain Gaussian noise.

Fig. 5 shows the diffusion coefficients D_{nn} and D_{ss} (shown in Fig.5 (a)), the Langevin forces FN and FS (shown in Fig. 5(b)), the optical noise (see Fig. 5(c)), and the noisy optical power $P_{opt\text{-}noise}$ (see Fig. 5(d)). We noted that $P_{opt\text{-}Noise}$ fluctuates because of the noise phenomenon and the GWN (Gaussian White Noise). It is equal to the sum of the output optical power and the optical noise P_{rin}, which can be calculated using the value of the relative intensity noise (RIN) provided by the VCSEL manufacturer [37].

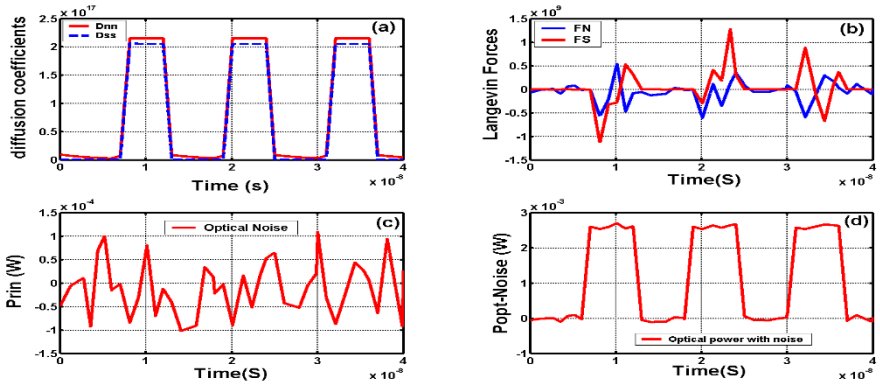

Fig. 5. Simulation results of the noise parameters disrupting the VCSEL output power. (a) The diffusion coefficients; (b) Langevin forces; (c) optical noise; and (d) output optical power with noise.

The VCSEL models that we created are very similar in terms of physics; they can aid in the design of a more efficient VCSEL by introducing several phenomena so we can arrive at the best accuracy/speed compromise for several applications. We integrated the noise sources in the same model of the VCSEL to avoid the maximum of overlap with the output optical power of the components. The simulation results were found to be favorable in comparison with other results published in the literature by several researchers.

IV. SIMULATION RESULTS FOR THE GRADED-INDEX AND STEP-INDEX FIBERS

Along the transmission in a system based on a fiber, the fiber performance decreases because of several phenomena, including attenuation and modal dispersion, which vary with the length of the transmission line. The fibers used in our study were graded-index and step-index fibers, which helped to consider the influence of attenuation and modal dispersion on the characteristics of the signal propagated. It was important to consider the effects of attenuation and modal dispersion in this model. The linear attenuation value, which is available on the data sheets from the manufacturer, was integrated into our model. This value is indicated by the decreasing rate of the average optical power with respect to the distance along the fiber.

The power at a distance L along the fiber can be described by $P(L) = P(0).10^{-A.(L/10)}$, where P (0) is the power at L = 0 and A is the attenuation coefficient reported in dB/km if L is in km [38]. The modal dispersion (τ_{mod} (Ps) = L.D_{mod} [39]) is the main cause of pulse enlargement in multimode optical fibers due to differences in the travel time of light rays. The modal dispersion coefficient of a graded-index fiber is expressed by D_{mod} (Ps / Km) = ($NA^4/8.n_c3.c$) [40] and that of a step-index fiber is expressed by D_{mod} (Ps / Km) = ($NA^2/2.n_c.c$), where NA is the numerical aperture and c is the speed of light. The total dispersion (τ_{tot}) [37] is the quadratic addition of the modal and chromatic dispersion due to their statistical effects on trips along the fiber.

4.1. Graded-index fiber modeling

To model the graded-index fiber, we used the following characteristics: a numerical aperture of 0.275, a wavelength of 1330 nm, a center refractive index of 1.5, a cladding refractive index of 1.474, a profile exponent of 2, a core radius (a) of 25 µm, a cladding radius and (b) of 60 µm, and an attenuation of 0.33 dB/Km. To study the refractive index profile across the GI-fiber, We wrote the fiber models in VHDL-AMS using the following equations:

$$n(r) = \begin{cases} n_c\left[1-2\Delta\left(\frac{r}{a}\right)^{\alpha}\right]^{\frac{1}{2}} & if\ r \le a \\ ng & if\ r > a \end{cases} \quad (1) \qquad \lim_{r \to a^-} n(r) = n_g \quad and\ n(0) = n_c \quad (2)$$

where $\Delta=\frac{n_c^2-n_g^2}{2n_c^2}$ is the index difference between the core and cladding, *r* is the radial distance from the fiber center, and α is the refractive index exponent. Note that the core grading becomes parabolic for α=2 [41].

The following program shows the first model of the graded-index fiber using the 'break' and 'dot' instructions to limit the radial distance between -25 and 25 µm and to trace it as straight. This model considers the change of the refractive index in three fiber regions: the core, the cladding and the vacuum. The second model studies the refractive index profile only in the fiber core.

Begin

Break r => -80.0e-6; -- initial value of the radial distance.

r'dot = = 40.0e+2;

If r <= - b or r >= + b Use $n_c(r) = = n_v$;

Elsif r >= - a and r <= + a Use $n_c(r) = = n_c(0)$*SQRT (1.0-((2.0*Δ)*(((r)/a)**α)));

Else $n_c(r) = = n_g$;

End use; End use;

The graded-index fiber core is composed of several layers of glass, each with a slightly different refractive index than the previous one, such that the core refractive index decreases from the propagation axis (r = 0) to the core-cladding interface. It is maximal at the core center for a value of n_{c0} = 1.5, and, at the core-cladding junction, it takes the value of the cladding refractive index (n_g = 1.474) according Figs. 6(a) and (b). The core refractive index takes the value of the vacuum refractive index (n_v = 1) at the cladding-vacuum junction (see Fig. 6 (a)).

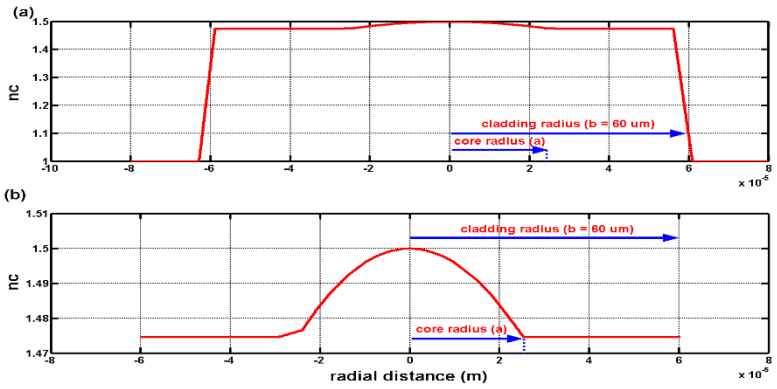

Fig. 6. Simulation result of the profile of the core refractive index for a graded-index fiber. (a) The variation of nc in the core-cladding-vacuum junctions and (b) the variation of nc in the core-cladding junction.

Theoretically, the cladding is not essential to the signal transmission. The rays can be guided by the silica core only because of its high refractive index compared than that of a vacuum. The importance of the cladding is to strengthen the fiber and prevent it from breaking or being damaged easily and prevents light leakage to other fibers.

The graded-index optical fiber modeled in this study used a wavelength of 1330 nm. Here, we assumed that the chromatic dispersion is zero, as explained in [42-44]. Fig. 7(a) and (c) show the modal dispersion coefficient and the modal dispersion for 1 Km of fiber length. We noted that the modal dispersion coefficient varies inversely with the core refractive index. The modal dispersion value τ_{mod} varies with its coefficient D_{mod} depending on the fiber length. The parameters D_{mod} and τ_{mod} are minimal in the fiber core center; they follow the curve of the core refractive index. As shown in Fig. 7(b), we noted the modal dispersion variation $\Delta\tau_{mod}/\Delta L$ = 0.7 ns/Km by assuming that D_{mod} remains constant

with the variation in the fiber length. Fig. 7(d) shows the total dispersion variation with the fiber length. This variation is equal to that of the modal dispersion because the chromatic dispersion is zero.

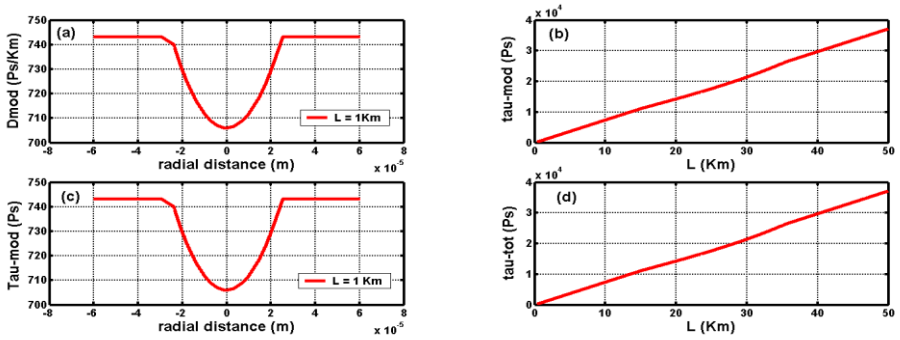

Fig. 7. Simulation results of the graded-index fiber. (a) The modal dispersion coefficient for L = 1 Km versus radial distance; (b) modal dispersion versus length; (c) modal dispersion for L = 1 Km versus radial distance; and (d) total dispersion versus length.

The bandwidth is inversely proportional to the fiber length, as shown in Figs. 8(a) and 9(c). The bandwidth variation with the fiber length for a graded-index fiber is illustrated in Fig. 8(a); it is equal to $\Delta Bp/\Delta L$ = -104 MHz/Km. Fig. 8(b) shows the product $B_P.L$, which follows a parabolic form varying between 592 and 623 MHz.Km.

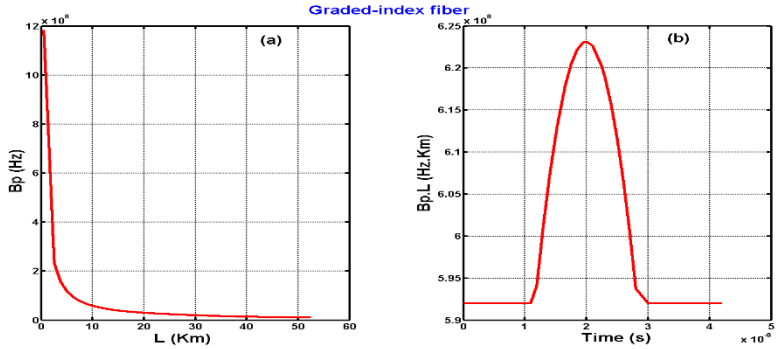

Fig. 8. Simulation results of the graded-index fiber. (a) The bandwidth variation versus length and (b) the product B_p.L versus time.

The main characteristics of the graded-index fiber can be related to its refractive index profile, such as the bandwidth, modal dispersion, propagation delay and coupling coefficients. For this, we considered the parabolic profile of the core refractive index in our fiber models.

4.2. Step-index fiber modeling

To model the step-index fiber, we use a numerical aperture of 0.36, a wavelength of 850 nm, a center refractive index (n_{c0}) of 1.492, a cladding refractive index of 1.436, and a core radius (a) of 50 µm. To model the step-index fiber with a wavelength of 850 nm, we use a chromatic dispersion coefficient of -46 Ps/nm/Km.

Fig. 9(a) shows that the core refractive index of the step-index fiber is constant over the fiber core diameter and then varies abruptly at the interface between the core and the cladding to reach the n_g value. Our results are consistent with those from other studies [45]. Fig. 9(b) shows that the modal dispersion follows a linearly profile because the refractive index remains constant in a step index fiber. The τ_{mod} augmentation with increasing fiber length is equal at Δtau-mod/ΔL = 151.55 ns/Km. In addition, the results show that the modal dispersion coefficient is constant for a value of 148.45 ns. The chromatic dispersion is equal to 46 Ps; it is negligible compared to the modal dispersion. Fig. 9(c) shows

the product BP.L and the bandwidth variation with the fiber length of the SI-fiber; notice that B_P.L is constant for a value of 10 MHz.Km and $\Delta B_p/\Delta L$ = -5 MHz/Km.

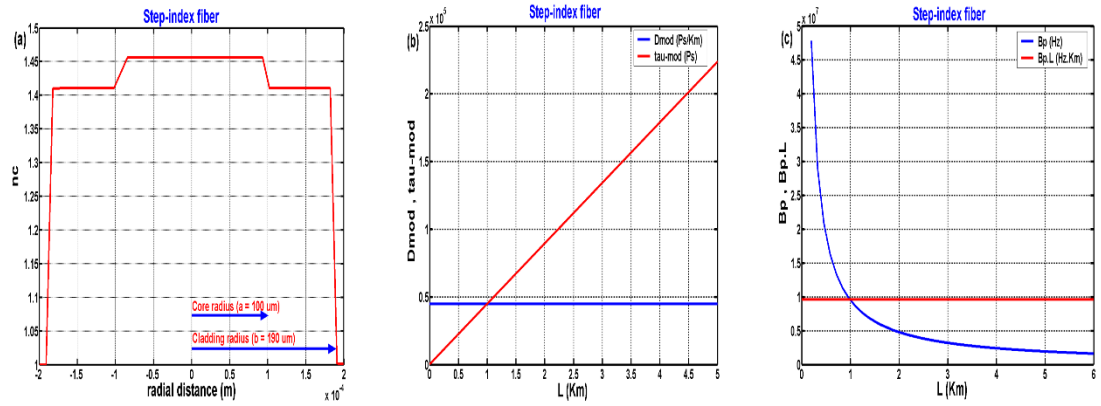

Fig. 9. Simulation results for the step-index fiber. (a) The core refractive index profile in the core-cladding-vacuum junctions; (b) dispersion parameters versus length; and (c) bandwidth and product B_p.L versus length.

Comparing the previous results, we conclude that the modal dispersion of a graded index fiber is lower than that of a step-index fiber.

4.3. Simulation results of the VCSEL-fiber coupling

To study the limits of the fiber, we wrote the VHDL-AMS models using the "DOT" command, which allows the representation of the fiber length as a straight line varying between 1 and 50 km for the GI-fiber and between 500 m to 6 Km for the SI-fiber.

The transmission system that we planned to simulate is comprised a transmitter, a transmission channel, and a receiver. In this study, our system was based on an electro-optical transmitter, which is a VCSEL laser diode, and a transmission medium, which is a multimode optical fiber.

To transmit the optical power through the fiber, it should connect the VCSEL and the fiber and the two fibers to consider the losses related to positioning inaccuracies between them. The ratio of the light received by the fiber to the light emitted from the VCSEL is called the coupling coefficient (η_c). The output power of the VCSEL-fiber-connector is given by $P_{out\_c} = P_{out\_F}.(10^{\frac{L_{tot}}{10}})$, where L_{tot} is the total length and P_{out_F} is the output power of the fiber. We wrote the connector models separately for the fiber model, and then we connected them using the "Test-Bench" option. For a better representation of our results, we did not account for the temporal lag between the input and output signals of the fiber due to the travel time.

Fig. 10 shows the simulation results of light transmission through the graded-index fiber and the step-index fiber, for several lengths. The optical powers represented are $P_{opt\text{-}VCSEL}$ for the VCSEL output, $P_{opt\text{-}C\text{-}VCSEL\text{-}F1}$ for the VCSEL-fiber-connector output, $P_{opt\text{-}F1}$ for the first fiber output, $P_{opt\text{-}C\text{-}F1\text{-}F2}$ for the fiber1-fiber2-connector output and $P_{opt\text{-}F2}$ the optical power to the second fiber output. We noticed that $P_{opt\text{-}VCSEL}$ and $P_{opt\text{-}VCSEL\text{-}C\text{-}F1}$ did not change as a function of the fiber length. In contrast, $P_{opt\text{-}F1}$, $P_{opt\text{-}C\text{-}F1\text{-}F2}$ and $P_{opt\text{-}F2}$ decreased with increasing fiber length while $P_{opt\text{-}F2}$ decreased to 1 µW for L = 50 km for the graded-index fiber, and, for the step-index fiber, it decreased to 2 µW for L = 6 km. We also noted that the fiber output power was attenuated and expanded compared to the input power emitted by the VCSEL laser, which is the result of the attenuation, the modal dispersion (which increases with distance traveled by the light), the loss due to the coupling and the fiber curvature. In Fig. 10 (a),(b), and (c), we observed that, for a GI-fiber length of 1 to 20 km, the signal was faithfully transmitted, which was not the case for a fiber length of 20 to 50 km, where the output signal begins to degrade. By performing several tests, we observed that the output signal was not reproducible against the input signal beyond 20 km. We also noted that $P_{opt\text{-}F2}$ of the graded-index fiber was attenuated compared to $P_{opt\text{-}VCSEL}$ due to the intrinsic attenuation of the optical fiber and the modal dispersion effect, which increased with the distance traveled. In Fig. 10 (d), (e), and (f), we see that, in the SI-fiber, the power was unreliable from 3 Km.

We noted a decrease of the optical power with an increase in the fiber length. The optical power began to disappear at 6 km of length.

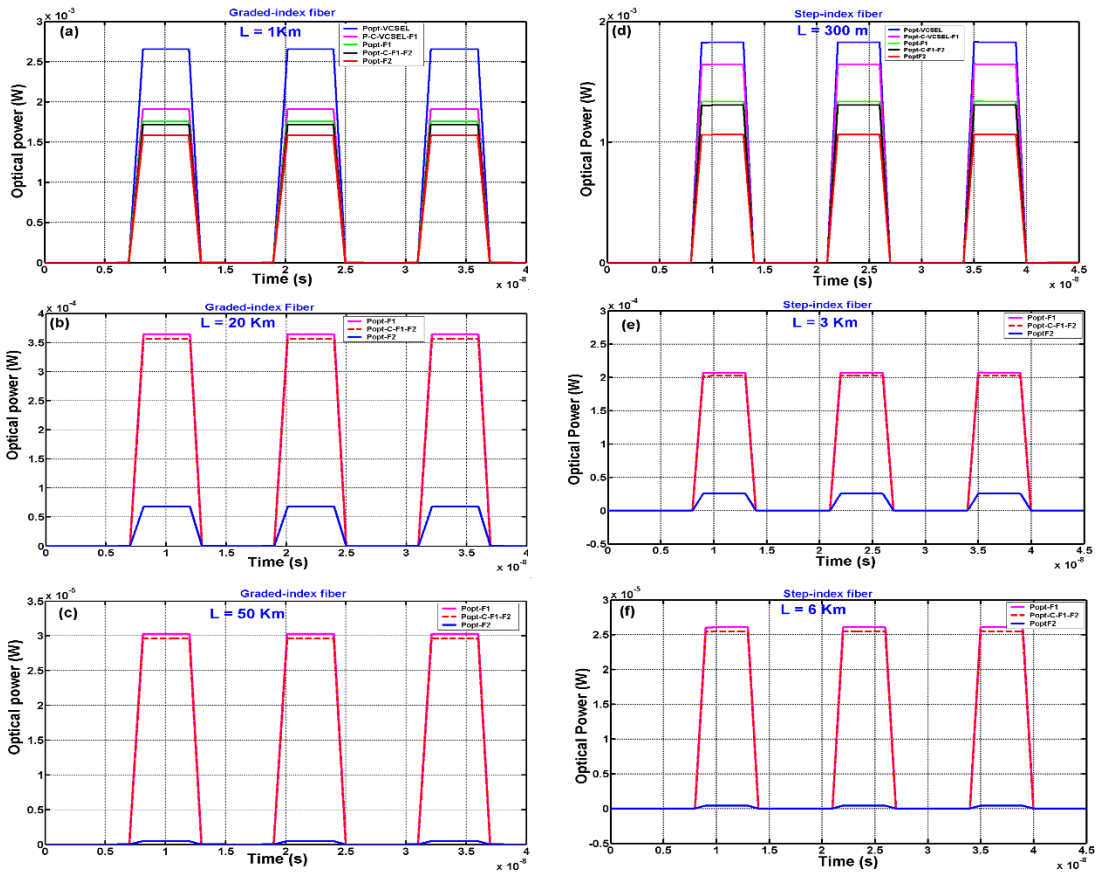

Fig. 10. Simulation results of the optical power through graded-index and step-index fiber versus time for different lengths values. (a) L (GI) = 1 Km; (b) L (GI) = 20 Km; (c) L (GI) = 50 Km; (d) L (SI) = 300 m; (e) L (SI) = 3 Km; and (f) L (SI) = 6 Km.

We can add the fiber and the coupling models to the library of optoelectronic components. Given our simulation results, we conclude that the GI-fiber is more advantageous compared to the SI-fiber. The parabolic profile of the core refractive index minimizes the modal dispersion of a GI-fiber, which reduces the signal propagation time. In a graded-index optical fiber, the velocity differences are much lower than those in a step-index fiber, which causes a smaller enlargement of the pulse. Our simulation makes it possible to optimize transmission and reception circuits.

V. CONCLUSION

We have presented a VHDL-AMS based methodology to modeling and simulation of mixed-technology which consist of electrical and optical circuits described by differential equations. We intentionally kept our examples straightforward to demonstrate clearly all steps involved into the modeling and simulation process. These examples demonstrate that VHDL-AMS is well suited for modeling and simulation of complex mixed-technology systems. This study provides many opportunities to assemble a rich library of reliable models for optoelectronic components. It is essential to provide generalization and model documentation [46].

In this paper, we have modeled the transmission physical phenomena of a VCSEL laser diode through two types of multi-mode optical fiber (Graded index and Step index). We have inserted disturbances parameters, such as noise through the VCSEL, temperature, optical fiber attenuation and chromatic dispersion and modal for knowing the transmission limitations according to the length of each fiber type. We developed several operational models using a well-documented generic VHDL-AMS library to design a complete transmission system based on the physical and technological knowledge of its

components. We have managed the configurations, the abstractions and their cohabitation and we studied the robustness and the parametric sensitivity while providing a process design that minimizes the risk industry. We have studied the optical power at the outputs of the two types of the multimode optical fiber according to the fiber length. The light signal was transmitted faithfully to the length of 50 Km in a graded index fiber and 6 km in a step index fiber where the signal begins to degrade until the total disappearance. Thus we can know the limitations of each type of fiber with respect to the length.
The perspective of this study is to develop other models of optoelectronic components by simultaneously combining the users and the manufacturers of components and to integrate our models into high-level modeling systems. For this we want to find the method to be able to integrate our models in a modern fiber-optic communications system such as Wavelength Division Multiplexing (WDM). We seek to model the five blocks: the transmitter block, the multiplexer, the optical amplifier, the demultiplexer and receiving block.

REFERENCES

[1] Mantooth H. A, Levy A, Francis A. M, Cilio E. S and Lostetter A. B, "Model-Based Design Tools for Extending COTS Components to Extreme Environments", AERO 2006; 1655977: 1-11.
[2] Hervé Y, « VHDL-AMS application et enjeux industriels », Dunod éditeur Paris 2002; ISBN 2100058886.
[3] Standards Board, "IEEE Standard VHDL-AMS analog and mixed-signal extensions", IEEE SA 2007; ISBN 0-7381-5627-2 SH 95694.
[4] Grimn C, Waldschmidt K, (1996) "KIR-Agraph-based model for description of mixed analog/ digital system", EURDAC, 10.1109/..558260, pp 568-573.
[5] Hartong W, Cranston S, (2009) "Real valued modeling for mixed signal simulation", product version IES, Vol. 8, No. 2, pp 1-20.
[6] Rouillard J, « Ecrire et comprendre VHDL-AMS », USA 2008, ISBN 978-1-4092-3689-4.
[7] Sorin A. Huss, "Model engineering in mixed-signal circuit design", Netherland 2001, ISBN 0-7923-7598-x.
[8] Degreys P, Hervé Y, Oudinot J, Snaidero S and Karray M, (2004) " SoC modelling for virtual prototyping with VHDL-AMS", Conf / fdl / HOSK04 Lille, pp 168-180.
[9] Herve Y, « VHDL-AMS un outil de l'électronique moderne », LAAS– ENSPS 2003, pp 1-13.
[10] Jridi M. Etude, modélisation et amélioration des performances des convertisseurs analogique numérique entrelacés dans le temps. Version 1 2008; n° order: 3517.
[11] Iga K, Koyama F, Kinoshita S, (1988) "Surface emitting semiconductor laser", IEEE J. Quantum Electron, Vol. 24, No. 9, pp 1845-1855.
[12] Iga K, (1998) "Surface emitting laser", Trans.IEICE, CI 1998; JB1-C-1 (9), pp 483-493.
[13] Karray M, Desgreys P, Charlot J-J, (2003) "VHDL-AMS modeling of VCSEL including noise", DOI.10.1109/BMAS.2003.1249869, pp 118-121.
[14] Toffano Z, Pez M, Desgreys P, Herve Y, et al., (2003) « Multilevel behavioral simulation of VCSEL based optoelectronic modules", IEEE journal of selected topics in quantum electronics,Vol. 9, No. 3, pp 949-960.
[15] Desgreys P, Karray M, Charlot J-J, Hervé Y, (2002) " Opto-Electro-Thermal model of a VCSEL array using VHDL-AMS", DOI. 10.1109/ BMAS.2002.1291070, pp 123-126.
[16] Karray M, Charlot J-J, Desgrys P, Pez M, (2004) " VHDL-AMS model of VCSEL emission module with thermal effects", BMAS, DOI. 10.1109/BMAS.2004.1393984, pp 64-67.
[17] Zei L-G, Ebers S, Kropp J-R, Petermann K, (2000) " Noise performance of multimode VCSELs", Journal of Lightwave Technology, Vol. 19, No. 6, pp 884-892.
[18] Mieyeville F, Jacquemod G, Gaffiot F, Belleville M. (2001) "A behavioural opto-electro-thermal VCSEL model for simulation of optical links", Sensors and Actuators, Vol. 88, No. 3, pp 209-219.
[19] Rissons A, Mollier J-C, Toffano Z, et al. Thermal and optoelectronic model of VCSEL arrays for short range communications. Proceedings of SPIE 2003; Vol. 4994, pp 100-111.
[20] Liu Jie, Chen Wen-lu, Li Yu-quan, (2006) "Rate-equation-based VCSEL thermal model and simulation", Journal of Zhejiang University SCIENCE ; DOI:10.1631/jzus.2006.A1968: Dc:A:CLC n°: TN2: 1968-72.
[21] Christopher J.O.Brien, Marian L.Majewski, Aleksandar D.Rakic, (2007) "A critical comparison of high-speed VCSEL characterization techniques", Journal of lightwave technology, Vol. 25, No2, pp 597- 605.
[22] Sherwin R.Sompie, Henri P.Uranus, (2011) " Design of single-transversal-mode VCSEL with photonic crystal holey cladding", DOI. 10.1109/ICEEI, 6021500, pp 1-5.
[23] Satuby Y, Orenstein M, (1998) "Small-signal modulation of multitransverse modes vertical-cavity surface-emitting semiconductor lasers", IEEE Photonics Technology Letters, Vol. 10, No 6, pp 757-759.
[24] Mena P. V, Morikuni J. J, Kang S. M, et al., (1999) "A simple rate-equation- based thermal VCSEL model", J. Lightwave Technol, Vol. 17, No 5, pp 865-872.

[25] Rissons A, Julien Perchoux J, Mollier J-C, Grabherr M, (2004) " Noise and signal modeling of various VCSEL structures", Proceedings of SPIE, Vol. 5364, pp 80-91.
[26] Blokhin S.A, Sakharov A.V, Maleev N.A, et al., (2006) "Experimental study of temperature dependence of threshold characteristics in semiconductor VCSELs based on submonolayer InGaAs QDs", ISSN 1063-7826 Semiconductors, Vol. 40, No 10, pp 1232-1236.
[27] Micro switch sensing and control, modulating VCSELs. Application Sheet, for application help: call 1-800-367-6786 Honeywell.
[28] Mena P. V, OSA, Morikuni J. J, Kang S.-M, Harton A. V, Wyatt K. W, (1999) "A comprehensive circuit-level model of vertical-cavity surface-emitting lasers", Journal of Lightwave Technology , Vol. 17, No. 12, pp 2612-2632.
[29] Prashant P. B, Benjamin K, Petter W, et al., (2011) "Assessment of VCSEL thermal rollover mechanisms from measurements and empirical modeling", Optics Express, Vol. 19, No. 16, pp 15490-15505.
[30] H.K. Lee, Y.M. Song, Y.T. Lee, J.S. Yu, (2009) "Thermal analysis of asymmetric intracavity-contacted oxide-aperture VCSELs for efficient heat dissipation", Solid-State Electronics, Vol. 53, pp 1086–1091.
[31] Gholami A, Toffano Z, Destrez Z, Pez M, Quentel F, (2006) "Spatiotemporal and thermal analysis of VCSEL for short-range gigabit optical links", Optical and Quantum Electronics, Vol. 38, pp 479–493.
[32] Agrawal G.P, Gray G.R, (1991) "Intensity and phase noise in microcavity surface-emitting semiconductor lasers", Appl. Phys. Lett, Vol. 59, No. 4, pp 399-401.
[33] S. F. Yu, (1999) "Nonlinear dynamics of vertical-cavity surface-emitting lasers", IEEE J. of Quantum Electronics, Vol. 35, No 3, pp 332-341.
[34] Michalzik R, Ebeling K.J, " Operating principles of VCSELs. University of Ulm: Optoelectronics Department Germany", D-89069 Ulm.
[35] Harder C, Katz J, Margalit S, et al., (1982) " Noise equivalent circuit of a semiconductor laser diode", IEEE Journal of Electronics, QE-, Vol. 18, No 3.
[36] Guy Van der Sande, Miguel C. Soriano, Mirvais Yousefi, et al., (2006) "Influence of current noise on the relaxation oscillation dynamics of semiconductor lasers", Applied physics letters, Vol. 88, No. 071107.
[37] Liu An-Jin, Qu Hong-Wei, Chen Wei, et al., (2011) "Graded index profiles and loss-induced single-mode characteristics in vertical-cavity surface-emitting lasers with petal-shape holey structure", Chin. Phys, Vol. 20, No. 2, pp 024204-1/-8.
[38] Yabre G, (2000) "Comprehensive theory of dispersion in graded-Index optical fibers", Journal of lightwave technology, Vol. 18, No. 2.
[39] Telecommunication standardization sector of ITU, characteristics of a 50/125 µm multimode graded index optical fiber cable. G.651 (02/98).
[40] IUT de Grenoble, (2010) « Reseaux and telecommunication transmission par fibre optique », RT tpopt10.doc-1.
[41] Ishigure T, Nihei E, Koike Y, (1996) "Optimum refractive-index profile of the graded-index polymer optical fiber, toward gigabit data links", Applied Optics 20 , Vol. 35, No. 12, pp 2048-2053.
[42] Gao J, Li X, Flucke J, Boeck G, (2004) "Direct parameter-extraction method for laser diode rate-equation model", Journal of Lightwave Technology, Vol. 22, No 6.
[43] Laurent J, (2004) «Communication optique à très haut débit, Conservatoires National des Arts et Metiers », Centre de Paris, Departement STIC, Examen probatoire spécialité electronique, pp 1-36.
[44] Kuwaki N, Ohashi M, (1989) "Waveguide dispersion measurement technique for single-mode fibers using wavelength dependence of mode field radius", Journal of Lightwave Technology, Vol. 7, No 6, pp 990-996.
[45] Castro E, Martin P, Puerta J, Cereceda C, (2006) " Guided-wave modes in graded-index optical fibers by two-point quasi-rational approximants", Revista Mexicana de Fisica; Vol. 52, No 2, pp 120-128.
[46] Milet-Lewis N, Snaidero S, Hervé Y, Monnerie G, et al., (2002) « Behavioural library development: models documentation and qualification", FDL'02.

AUTHOR'S BIOGRAPHY

BAOUCHE FATIMA ZOHRA received her Magister degree in Electronics from "Université Mentouri de Constantine–Algeria" in 2005. Currently she is pursuing his PhD degree working with the laboratory of instrumentation and microelectronics (LMI) at University of Constantine-Algeria in collaboration with InESS laboratory at University of Strasbourg. Presently she is teacher at the University of Khemis Miliana-Algeria since 2006. Her special field of interest is the VHDL-AMS modeling of the multidisciplinary systems.

HOBAR FARIDA obtained her Ph.D in Electronics from "Université de Toulouse-France" in 1983. Currently she is Professor at University of Constantine-Algeria and Vice-Rector for External Relations, Cooperation, animation and communication and Scientific Events at university of Constantine-Algeria. Her research interests include topics on Nano-electronics VHDL-AMS modeling of the multidisciplinary systems.

YANNICK HERVE received the Aggregation degree from "Ecole Normale Supérieure" in Electrical Sciences in 1985, the PhD degree in Computer Science and Electronics in 1988 and Habilitation in research Management degree in 2003. He is associate professor at the "Université de Strasbourg-France". His research work, in the field of methods, languages and tools for virtual prototyping, is within the Department of Complex Systems Modeling and Simulation at the InESS-UMR 7163 Laboratory in Strasbourg, France. He was the initiator "SimFonIA" Company. He is scientific advisor for several companies in complex system design and associated methodologies and tools.